 DOI: 10.1002/eji.201445307 Eur. J. Immunol. 2015. 45: 1248–1257

European Journal of Immunology

F pocket flexibility influences the tapasin dependence of two differentially disease-associated MHC Class I proteins

Esam T. Abualrous[1,2], Susanne Fritzsche[1], Zeynep Hein[1], Mohammed S. Al-Balushi[1,3], Peter Reinink[1,4], Louise H. Boyle[5], Ursula Wellbrock[1], Antony N. Antoniou[6] and Sebastian Springer[1]

[1] Department of Life Science and Chemistry, Jacobs University Bremen, Bremen, Germany
[2] Department of Physics, Faculty of Science, Ain Shams University, Cairo, Egypt
[3] Department of Microbiology and Immunology, Sultan Qaboos University, Muscat, Oman
[4] Department of Infectious Diseases and Immunology, Faculty of Veterinary Medicine, Utrecht University, Utrecht, The Netherlands
[5] Division of Immunology, Department of Pathology, Cambridge University, Cambridge, UK
[6] University of East London, London, UK

The human MHC class I protein HLA-B*27:05 is statistically associated with ankylosing spondylitis, unlike HLA-B*27:09, which differs in a single amino acid in the F pocket of the peptide-binding groove. To understand how this unique amino acid difference leads to a different behavior of the proteins in the cell, we have investigated the conformational stability of both proteins using a combination of in silico and experimental approaches. Here, we show that the binding site of B*27:05 is conformationally disordered in the absence of peptide due to a charge repulsion at the bottom of the F pocket. In agreement with this, B*27:05 requires the chaperone protein tapasin to a greater extent than the conformationally stable B*27:09 in order to remain structured and to bind peptide. Taken together, our data demonstrate a method to predict tapasin dependence and physiological behavior from the sequence and crystal structure of a particular class I allotype.

Keywords: Ankylosing spondylitis · HLA-B27 · Major histocompatibility complex · Molecular dynamics · Natively unstructured proteins · Protein folding · Simulations

Additional supporting information may be found in the online version of this article at the publisher's web-site

Introduction

MHC class I molecules are heterotrimeric proteins that transport antigenic peptides to the cell surface and present them to cytotoxic T cells. They consist of the transmembrane heavy chain (HC), the noncovalently associated light chain beta-2 microglobulin (β_2m), and an antigenic peptide of eight to ten amino acids. The extracellular part of the heavy chain comprises the α_1, α_2, and α_3 domains. The α_1 and α_2 domains form the peptide-binding groove, a superdomain that consists of an antiparallel beta sheet surmounted by two alpha helices, between which the peptide binds [1, 2].

In the cell, peptide binding to class I is a multistep process within the ER. It involves the peptide-loading complex, which consists of the peptide transporter associated with antigen processing (TAP) that transports peptides from the cytosol into the ER lumen [3] and several chaperone proteins such as tapasin, which binds both to the class I molecule and TAP [4, 5].

Correspondence: Prof. Sebastian Springer
e-mail: s.springer@jacobs-university.de

The sequence of peptides that can bind to class I is determined by interactions with the amino acid side chains of the peptide-binding groove. The high sequence polymorphism of the peptide-binding groove in human class I molecules (human leukocyte antigens, HLA-A, -B, and -C) means that different allotypes bind different peptides; thus, individual HLA allotypes—such as HLA-B27–support-specific immune responses and are statistically associated with disease [6, 7]. Among the subtypes of HLA-B27 [8, 9], HLA-B*27:05 (B*27:05) shows a very strong statistical association with spondyloarthropathies such as ankylosing spondylitis (AS), in contrast to HLA-B*27:09 (B*27:09), which does not [10–12]. The two subtypes differ only in a single residue at position 116 (histidine in B*27:09 and aspartate in B*27:05) at the bottom of the F pocket, which binds the side chain of the C-terminal amino acid of the peptide [13]. How this single amino acid difference causes the striking difference in disease association is not understood, despite intense investigation; one prominent hypothesis states that an inherent folding inefficiency of B*27:05 triggers a cellular response that leads to inflammation [9, 14]. So far, studies have mostly focused on identifying conformational and dynamic features that distinguish B*27:09 and B*27:05 [12, 15, 16].

The F pocket region, i.e. the end of the binding groove that includes the F pocket, is the proposed binding region of tapasin, according to experimental, and theoretical investigations [17–20]; but as yet, no crystal structure of a complex between class I and tapasin exists. In cells, tapasin reduces the conformational disorder of empty or suboptimally loaded class I molecules, and it mediates iterative peptide exchange by accelerating dissociation [1, 21–23]. Many class I allotypes require tapasin for any binding of high-affinity peptides and subsequent surface transport and are thus termed tapasin-dependent; others do not, or to a lesser degree. With regard to the tapasin dependence of the B27 subtypes, conflicting reports exist [22, 24–28], and generally, it is not well understood what makes a particular class I allotype tapasin-dependent or –independent [21].

In this work, we have compared the conformational stabilities of the B*27:05 and B*27:09 subtypes through a combination of in silico, biochemical, and cellular approaches. We find that the disease-associated B*27:05 is much more conformationally disordered than B*27:09 in the empty and suboptimally loaded states, and that it requires tapasin, at least to a large extent, for its surface expression. Our results establish a general molecular reason for the tapasin dependence of MHC class I molecules and demonstrate tools for its in silico prediction.

Results

The conformational flexibility of the binding groove in silico differs between HLA-B27 subtypes

To understand the differences in structure and dynamics between B*27:05 and B*27:09 due to the amino acid 116 variation, we analyzed whether the binding grooves of the subtypes exhibit different conformational flexibilities. We used published crystal structures [13] of the lumenal domains of B*27:05 and B*27:09 bound to the high-affinity peptide IRAAPPPLF (single-letter amino acid sequence; abbreviated as IF9; complexes abbreviated as B*27:05/IF9 and B*27:09/IF9) to build computational models of the empty peptide-binding grooves (empty B*27:05 and empty B*27:09). We then performed two independent molecular dynamics (MD) simulations for the entire heavy chain (α_1, α_2, and α_3 domains) and β_2m of each of these four structures, and we measured the root mean square deviation (RMSD, a measure of the overall conformational change away from the crystal structure) for the binding groove only (the α_1/α_2 superdomain, i.e. residues 1–180). The probability distribution of the RMSD values showed narrow peaks for B*27:05/IF9 and B*27:09/IF9 in both simulations (Fig. 1; solid black and gray). In contrast, the binding groove of empty B*27:05 showed much higher RMSD averages (Fig. 1, dashed black). Thus, the lack of full-length peptide altered the shape of the binding groove of B*27:05, most likely conformationally destabilizing it, as reported before [21, 29–31]. In surprising contrast, the binding groove of empty B*27:09 showed narrow peaks very close to those of the peptide-bound structures (Fig. 1, dashed gray), suggesting that the removal of the peptide did not significantly change the structure nor increase the flexibility of its binding groove. Thus, the histidine residue 116 at the bottom of the F pocket of B*27:09 supports a stable conformation of its binding groove, whereas the aspartate in the same position of B*27:05 contributes to destabilizing the conformation of the peptide-free protein.

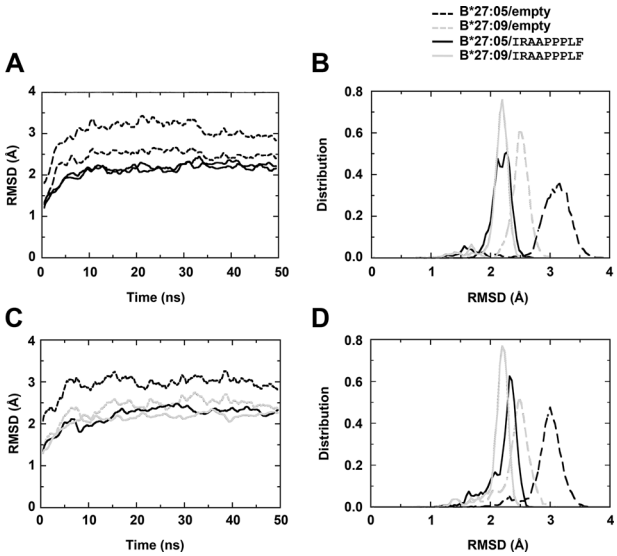

Figure 1. Root mean square deviation (RMSD) of the binding grooves (residues 1-180) of B*27:05, and B*27:09, both empty or in complex with IF9 peptide. Two independent sets of simulations (A/B and C/D) are shown as (A and C) RMSD time courses (moving average) and as (B and D) RMSD probability distributions.

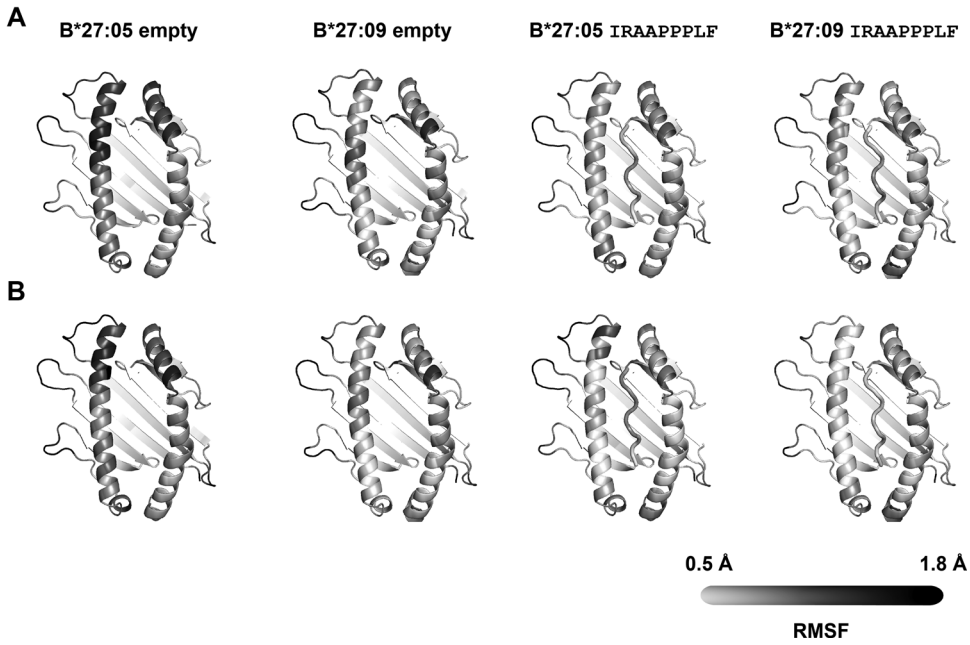

Figure 2. Conformational flexibility of individual residues (root mean square fluctuation, RMSF) of the binding grooves of B*27:05, and B*27:09, both empty or in complex with IF9 peptide. Two independent sets of simulations are shown (A and B). The RMSF value is calculated for each residue and depicted as a level of gray on a cartoon representation of the crystal structure of HLA-B*27.

The conformational fluctuation of B*27:05 is mostly in the F pocket region

To understand whether the conformational flexibility of the empty B*27:05 identified in Fig. 1 is focused on a particular region of the binding groove, we investigated the flexibility of individual residues by depicting the root mean square fluctuation of each residue on a gray scale, with darker gray meaning higher fluctuation (Fig. 2). The binding groove of empty B*27:05 showed very high flexibility in the F pocket region and along the α_1 helix, whereas for empty B*27:09, the fluctuation was low and not much different from peptide-bound B*27:05/IF9 and B*27:09/IF9. Thus, Asp116 at the bottom of the F pocket creates localized conformational disorder at that region of the empty B*27:05 molecule, which can be overcome by the binding of peptide, whereas B*27:09 is conformationally stable in both the empty and the peptide-bound forms.

The binding groove width of empty B*27:05 varies

We next wondered whether empty B*27:05 shows the variation of the binding groove width in silico that is a hallmark of conformationally disordered and tapasin-dependent class I molecules such as B*44:02 [21, 31]. To quantify width variation on a local scale, we divided the binding groove into three regions: region I, which contains the A pocket (Fig. 3A; residues 50–59 in the α_1 helix and 165–176 in the α_2 helix); region II, in the center of the binding groove (residues 60–72 and 152–164); and region III (above termed the F pocket region; residues 73–84 and 139–150). For each region, we then measured how the distance of the centers of mass varied during the simulation. In both subtypes, the peptide-bound binding groove showed the lowest width variation, similarly to published data [5, 32]. Empty B*27:09 showed an intermediate width variation between that of the empty B*27:05 and peptide-bound complexes, especially in regions II and III, as

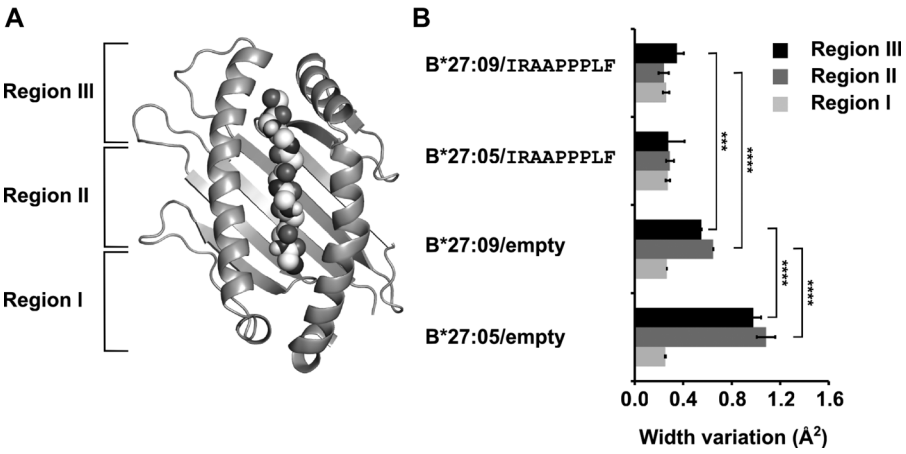

Figure 3. Width variation of HLA-B*27 binding groove. (A) Top view of class I. The binding groove was divided into three regions (see the text). (B) Width variation of each region of the binding groove was calculated from frames of two independent MD simulations of B*27:05 and B*27:09 with or without IF9 peptide. Error bars represent standard deviation. Significance **** $p < 0.0001$; unpaired two-tailed *t*-test.

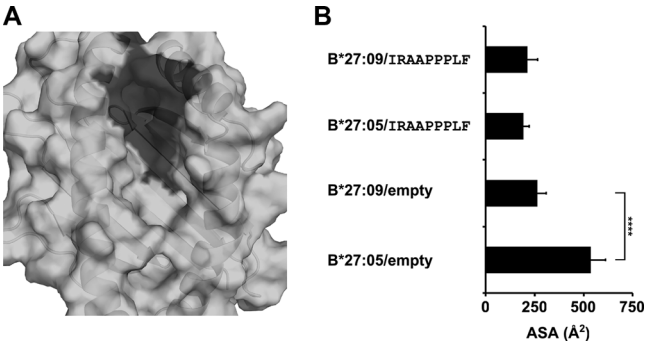

Figure 4. Solvent-accessible surface area of HLA B*27 during the simulations (A) molecular surface of the F pocket region depicted in dark gray on the B*27-binding groove. (B) Accessible surface area (ASA) of the F pocket region (residues Asp74, Asp77, Thr80, Leu81, Tyr84, Leu95, Asn97, His114, His/Asp116, Tyr123, Thr143, Lys146, Trp147) of B*27:05 and B*27:09 with or without IF9 peptide calculated from two independent simulations. Error bars represent standard deviation. **** $p < 0.0001$; unpaired two-tailed *t*-test.

reported for several empty murine and human allotypes [21, 29]. In contrast, for empty B*27:05, width variation of regions II and III was much higher than for B*27:05/IF9 and for empty B*27:09 (Fig. 3B). Thus, just like empty B*44:02 [21], empty B*27:05 appears to be conformationally disordered, even on the short-time scale of MD simulations and especially around the F pocket region.

B*27:05 has a higher solvent-accessible surface area during the simulation

We next hypothesized that if empty B*27:05 was indeed more conformationally disordered than empty B*27:09, it should expose a larger proportion of its F pocket to the solvent. To test this, we measured the solvent-accessible surface area (SASA) during the MD simulation using a probe radius of 1.4 Å, equivalent to that of a water molecule. In agreement with our hypothesis, the SASA of empty B*27:05, with 520 Å^2, was twice as high as that of empty B*27:09 (Fig. 4). Taken together with the data above, the increased SASA suggests that over the course of the simulations, the conformational flexibility of B*27:05 results in more conformational disorder and partially unfolded states of its binding groove. This suggests that B*27:05 might need tapasin to stabilize a conformation that can bind peptide.

B*27:05 is more tapasin-dependent than B*27:09 for surface transport

For the HLA-B44 subtypes HLA-B*44:02 and B*44:05, which also differ only in amino acid 116, the conformational flexibility of the empty peptide binding groove in silico correlates with tapasin dependence: empty B*44:02 is conformationally disordered and tapasin-dependent, whereas empty B*44:05 is conformationally stable and tapasin-independent [21, 33]. We thought

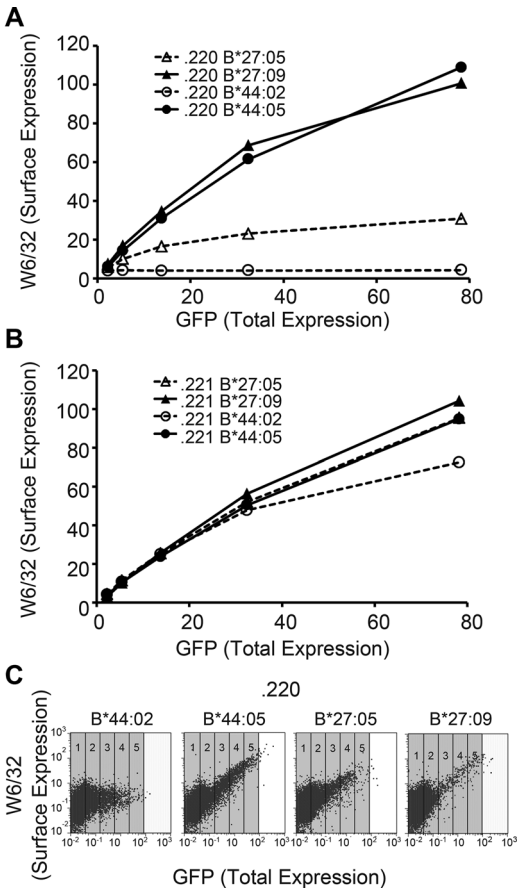

Figure 5. Analysis of surface level of HLA-B allotypes. (A and B) Tapasin-deficient LCL (A) 721.220 and (E) 721.221 cells were transiently transfected with the indicated HLA-B heavy chains fused to GFP. Surface molecules were detected by flow cytometry using MAb W6/32. (C) Key to the quantification and original flow cytometry data. The area of the scatter plots displaying GFP (*x* axis) versus W6/32 (*y* axis) fluorescence was divided in five vertical sectors containing no less than 100 events in each (note that the axes are on logarithmic scale in contrast to the graphs in A and B).

that this might be paralleled in the B27 subtypes, and so we next investigated their tapasin dependence. In the literature, B*27:05 was shown to exist at the surface of tapasin-deficient cell lines with peptides different from those of B*27:09 [25–27]. To directly compare how surface transport of B*27:05 and B*27:09 depends on tapasin, we transiently expressed both proteins as green fluorescent protein (GFP) fusions in tapasin-deficient human LCL721.220 (.220) cells. In the diagram in Fig. 5A, we show the surface levels of B*27:05 and B*27:09 in several brackets of gene expression (determined by GFP levels; original data in Fig. 5C). B*27:09 showed very high surface levels, just as B*44:05 [21, 22], whereas B*27:05 was detected at lower levels at the surface in both flow cytometry and microscopy (Fig. 5A and Supporting Information Fig. 1A and B). Importantly, B*27:05 levels were still higher than those of the tapasin-dependent allotype B*44:02, which demonstrates that B*27:05 is partially tapasin-dependent. In agreement with these findings, our microscopy analysis confirmed that in the same cells, the majority of B*27:05 resided in

the ER (with or without fused GFP), whereas B*27:09 was located at the cell surface almost exclusively (Supporting Information Fig. 1A and B). As a control, we expressed the same constructs in syngeneic tapasin-proficient LCL721.221 cells, where all showed the same surface levels; this confirms that the B*27:05 construct was fully functional Fig. 5B). Thus, in these two B27 subtypes, just as in B44, the relative tapasin-dependence of B*27:05 correlates with molecular disorder and flexibility of the empty peptide-binding site. Our observation of the partial tapasin dependence of B*27:05 agrees with the observations of others who found it on the surface of tapasin-deficient cells.

In the absence of peptide and tapasin, B*27:05 is partially unfolded

In live cells, the tapasin-dependent B44 subtype B*44:02 is unstructured and partially unfolded in the absence of tapasin and peptide [21]. To investigate whether B*27:05 has similar properties, we stably expressed B*27:05 and B*27:09 in murine CMT64.5 cells, which lack both tapasin and the TAP peptide transporter [34]. We lysed the cells and precipitated with the β_2m-dependent HLA-specific antibody W6/32. Interestingly, a major portion of B*27:09 was precipitated, but only a small fraction of B*27:05 (Fig. 6A). This suggests that without peptide and tapasin, B*27:05 cannot stably bind murine β_2m and is thus structurally unstable. When human β_2m was overexpressed in CMT64.5, a major fraction of B*27:05 was recovered as β_2m complex, demonstrating that the B*27:05 heavy chain was not irreversibly denatured. Just like in .220, B*27:05 was barely present at the surface of CMT64.5 cells, in contrast to B*27:09, suggesting that it was not sufficiently conformed to pass the cellular quality control (Fig. 6B) [35]. In agreement with this observation, most B*27:05 molecules in CMT64.5 cells were EndoF1-sensitive (i.e. confined to pre-Golgi compartments) at steady state, whereas most B*27:09 molecules were EndoF1-resistant (i.e. located at the cell surface; Fig. 6C). These results strongly support the notion that B*27:05 is intrinsically structurally disordered when no high-affinity peptide is available.

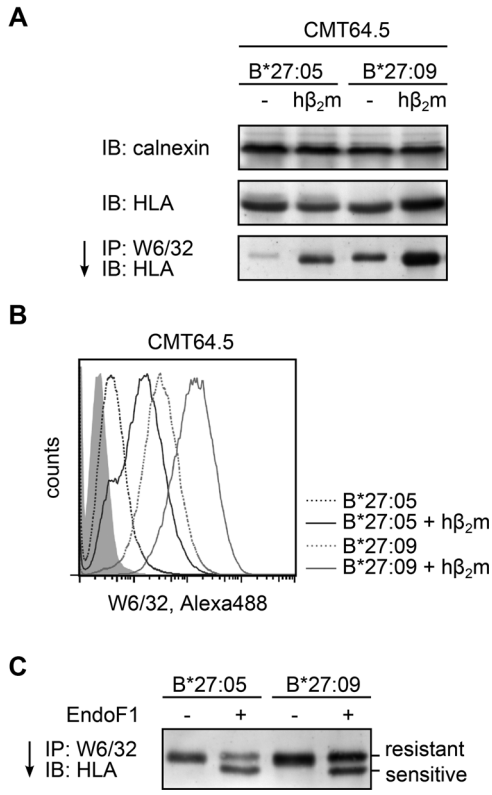

Figure 6. Analysis of the folding and stability of HLA-B allotypes (A) total cell lysates of murine CMT64.5 cells stably expressing B*27:05 or B*27:09 with or without additional human β_2m (hβ_2m) were separated by SDS-PAGE and immunoblotted (IB) for calnexin and HLA. An equal number of these cells was first subjected to immunoprecipitation (IP) with W6/32, separated by SDS-PAGE and immunoblotted using the anti-HLA serum. Representative gels out of three independent experiments are shown. (B) CMT64.5 cells stably expressing B*27:05 or B*27:09 with or without additional hβ_2m were stained with MAb W6/32 for surface HLA. (C) CMT64.5 cells stably expressing B*27:05 or B*27:09 and hβ_2m were lysed and HLA molecules immunoprecipitated with W6/32, then digested or mock-digested with EndoF1, and separated by SDS-PAGE. Immunoblotting was performed using anti-HLA serum. A representative gel out of two independent experiments is shown.

Protonation state of residue 116 resolved from MD simulations

To find the cause of the molecular disorder of B*27:05 compared with B*27:09, we analyzed the crystal structures. Both His116 and Asp116 at the bottom of the F pocket form a network of hydrogen bonds and salt bridges with residues of the α_1 and α_2 helices, and with the C-terminal amino acid side chain of the peptide [13, 36]. We hypothesized that in the absence of peptide from the B*27:05 binding groove, the neighboring acidic residues Asp116, Asp77, and Asp74 might repel each other and establish a negative electrostatic potential at the bottom of the F pocket. In empty B*27:09, in contrast, the imidazole group of His116 might prevent this repulsion and thus stabilize the conformation of the F pocket region. To clarify this effect, we simulated B*27:09 with different protonation states of His116.

Histidine residues in proteins have three different protonation states at physiological pH, depending on whether Nε, Nδ, or both nitrogens are protonated. They cannot be derived from the crystal structure. To determine the protonation state of His116, we thought to use the observation that the actual protonation state shows the lowest RMSD value of the histidine side chain and the surrounding residues in a MD simulation [37]. We thus performed two independent MD simulations of empty B*27:09 and B*27:09/IF9 for each possible protonation state. In the absence of peptide, we observed the lowest RMSD values when Nε only was protonated (Supporting Information Tables 1 and 2). In the presence of IF9, in contrast, the doubly protonated state appeared to be preferred. The same protonation states of His116 were suggested by the PROPKA server [38]. The protonated Nε of His116 in the empty B*27:09 can indeed form a hydrogen bond

with Asp77 (Supporting Information Fig. 2). For empty B*27:05, the RMSD values of the surroundings of Asp116 were higher than those of any of the three protonated states of His116 in B*27:09, again confirming its molecular disorder even on the short time scale of an MD simulation.

Taken together, the data suggest a molecular mechanism for the conformational disorder of B*27:05 and its difference to B*27:09. In the latter, His116 bonds to the surrounding residues, whereas in the former, Asp116 causes electrostatic repulsion and disorder. The binding of peptide supersedes these differences, and both subtypes have stably ordered conformations.

Discussion

Since B*27:05 and B*27:09 differ by only one amino acid and yet are differentially associated with ankylosing spondylitis, the molecular and cellular differences between the two subtypes have been intensely investigated [31, 36, 39–42]. We have focused here on comparing their conformational stabilities through a combined theoretical and experimental investigation.

All our data support the hypothesis that due to the repulsion between Asp116 and the acidic residues Asn97, Asp77, and Asp74, the F pocket region of B*27:05 shows a strong conformational fluctuation, whereas in B*27:09, His116 contributes to neutralizing the negative electrostatic potential of the environment and thus promotes conformational stability. Similar connections between electrostatic potential and the conformational flexibility of the binding groove have been proposed by others [31, 43].

We present evidence that this conformational fluctuation of B*27:05 in the empty state leads to its partial unfolding. The MD simulations, on a timescale of nano- to microseconds, are too short to observe protein unfolding (which occurs in milliseconds), but the biochemical data in Figs. 5 and 6, and Supporting Information Fig. 1 show that suboptimally loaded B*27:05 has difficulties to tightly bind β_2m and pass the cellular conformational quality control. We recently have shown that the conformational restriction of the F pocket region by a disulfide bond (C84-C139) helps the binding of β_2m to the heavy chain through conformational and dynamic effects that stabilize the folded conformation of class I and help it pass ER quality control [44].

In agreement with our findings, the recent nuclear magnetic resonance spectroscopy work of Kurimoto et al. suggests that in the absence of peptide, on a long timescale, the α_1 and α_2 domains of HLA-C may become entirely unfolded, with only the α_3 domain remaining structured [45]. The propensity of newly synthesized B*27:05 to misfold and aggregate has long been suggested to correlate with AS etiology [46–49].

With a partially unfolded binding site, a class I molecule would find it difficult to bind peptide. We have therefore proposed earlier that some empty or suboptimally loaded class I molecules require tapasin to maintain a structured peptide binding site, and thus to bind peptide [21, 44]. In keeping with this hypothesis, B*27:05 showed strong (but not absolute) tapasin dependence for surface transport in our quantitative analysis (Fig. 5, Supporting Information Fig. 1). Others have also shown that a substantial proportion of B*27:05 remains inside the cells, most likely due to deficiencies in folding [50, 51]. We still detected some B*27:05 on the surface of the .220 cells, which explains earlier reports that B*27:05 is not tapasin dependent [25–28]. The partial tapasin dependence of B*27:05 that we report here resembles that of HLA-A*02:01, which can bind to ER signal sequences and reach the cell surface in the absence of TAP and tapasin [52, 53]. In contrast to A*02:01; however, our observations (Fig. 6) and several other studies show that surface expression of B*27:05 does depend on the availability of peptides transported by TAP [54–57]. In the absence of tapasin, TAP-mediated peptide transport is generally assumed to function, but the stability and function of TAP is likely to be compromised [58, 59]. Thus, class I molecules expressed in tapasin-deficient cell lines are confronted with a different pool of peptides than in wild-type cells. In tapasin-deficient cells, both A*02:01 and B*27:05 can assemble with β_2m and some peptides, but the stability of the resulting trimeric complexes is low [22, 25, 60–62].

Taken together with our earlier work on B44 subtypes, our data suggest that tapasin not only exchanges peptides on class I molecules (as widely appreciated in the literature), but that its other and very important function is to help structure class I molecules such that they can bind peptide in the first place (see also [61, 63]). The higher the degree of molecular disorder in the absence of peptide (or in the suboptimally loaded state) for a specific class I allotype, the greater its dependence on tapasin for folding of the peptide-binding groove, for peptide binding, and thus for passing intracellular quality control and for surface expression.

From the comparison with B*44:02, which exhibits greater molecular disorder and greater tapasin dependence than B*27:05, our results now demonstrate that the molecular disorder of B*27:05 alone is not sufficient to explain its molecular pathology and disease association. To cause disease, B*27:05 must have additional other properties, such as homodimerization and/or induction of the unfolded protein response [16, 51, 64], which other conformationally disordered class I allotypes, such as B*44:02, lack.

Our work on the B27 and B44 subtypes demonstrates that tapasin dependence (the ability to form stable peptide-heavy chain-β_2m complexes without tapasin interaction) of an HLA molecule correlates with molecular disorder in the empty state. Thus, we propose that the degree of tapasin dependence of the thousands of biochemically uncharacterized HLA allotypes may in the future be predicted from observing molecular disorder by using in silico molecular dynamics simulations. Other properties that differ between HLA molecules, such as rate of surface transit [65] or inhibition of progression to viral disease [66], may also be directly or indirectly correlated with their conformational dynamics through mechanisms yet unknown, whose elucidation will require substantial experimental effort.

Materials and methods

Molecular dynamics simulations

The crystal structures of HLA-B*27:05 and HLA-B*27:09 in complex with the high-affinity peptides IRAAPPPLF (PDB ID code 3BP4 and 3BP7 [13]) served as the starting structure for the MD simulations. The empty structure was prepared by deleting the corresponding peptide residues from the crystal structure. With the Amber 12 simulation package [67], each complex was initially placed in an octahedral TiP3 [68] water box together with ten Na^+ and Cl^- ions and neutralized with eight counter-ions. Then, each complex was energy minimized, positionally restrained (25 kcal mol^{-1} $Å^{-2}$), and heated from 100 to 300 K. The restraints were resolved in five steps, and then each complex was equilibrated for 1 ns and simulated for 50 ns (12 500 frames). Short-range nonbonded interactions were taken into account up to a cut-off value of 9 Å. Long-range electrostatic interactions were treated with the particle mesh Ewald method [69]. The RMSD of residue His/Asp116 and its surroundings (Supporting Information Fig. 2) was measured with the RMSD trajectory tool of visual molecular dynamics [70]. The protein accessible surface area measurements were performed using the Protein Structure and Interaction Analyzer [71]. Visualization of trajectories and preparation of figures were performed using visual molecular dynamics and Pymol [70, 72].

Cell lines

Murine CMT64.5 cells were a kind gift of Hartmut Hengel (Düsseldorf, Germany). Anti-HLA antiserum H300 was purchased from Santa-Cruz Biotechnology (Dallas, TX, USA). Anti-calnexin serum was obtained from David B. Williams (Toronto, Canada). Monoclonal antibody W6/32 was produced in a hybridoma cell line received from Alan Townsend (Oxford, UK). Secondary antibody Alexa488, anti-rabbit and anti-mouse alkaline phosphatase conjugated secondary antibodies were purchased from Dianova GmbH (Hamburg, Germany).

Plasmids

HLA-B*27:05, HLA-B*27:09, HLA-B*44:02, and HLA-B*44:05 heavy chains were expressed from the pEGFP-N1 (Clontech, CA) backbone. Where mentioned, N-terminal HA-tagged versions of the allotypes on the same pEGFP-N1 backbone were used. Insertion of the HA tag was accomplished by a site directed mutagenesis method developed by Stratagene (Agilent Technologies, CA). LCL721.220 cells were grown in RPMI medium complemented with 10% fetal calf serum, 0.5 U/mL penicillin, and 0.1 μg/mL streptomycin (GE Healthcare Life Sciences, Freiburg, Germany). Cells were maintained at 37°C in 5% CO_2 atmosphere. Transfection by electroporation was modified from Majoul et al. [73]. Briefly, cells were washed twice with PBS and transferred into the transfection medium (120 mM KCl, 10 mM KH_2PO_4, 5 mM $MgCl_2$, 0.15 mM $CaCl_2$, 25 mM HEPES, pH 7.2, 2 mM EGTA, 2 mM ATP, and 5 mM oxidized glutathione). Five million cells were transfected in 500 μL final volume with 50 μg of maxiprep DNA (Qiagen, Hilden, Germany). Cells were electroporated by two pulses of 500 V for 2 ms and resuspended immediately in growth medium. Experiments were performed 24-36 h posttransfection.

Immunoprecipitations

Immunoprecipitations were performed by solubilization of the target cells in native lysis buffer (50 mM Tris pH 7.5, 150 mM NaCl, 5 mM EDTA, 1% Triton X-100) in the presence of 1 mM phenylmethylsulfonylfluoride and 5 mM iodoacetamide protease inhibitors for 1 h at 4°C. The lysates were subjected to preclearing with insoluble protein A for 30 min at 4°C, then transferred to antibody-bound protein A agarose beads and rotated for 1 h at 4°C. Subsequently, the beads were washed three times in wash buffer (50 mMTris pH 7.5, 150 mM NaCl, 5 mM EDTA, 0.1% Triton X-100) and used directly for SDS-PAGE, or treated with endoglycosidase F1 beforehand.

Total cell lysates were prepared from cells by denaturation in SDS-PAGE sample buffer (350 mM Tris-Cl pH 6.8, 36% glycerol, 10% SDS, 0.6 M DTT, 0.012% bromphenol blue in ethanol) at 95°C for 10 min.

Endoglycosidase F1 digests

Immunoprecipitates were digested with endoglycosidase F1 (EndoF1) by denaturation in 0.05% SDS, 0.1% 2-mercaptoethanol at 95°C for 10 min. The chilled samples were supplemented with 5 mM sodium citrate (pH 5.5) and 1% Triton X-100. For the digest, 1 μg of EndoF1 was added to each sample and incubated for 1 h at 37°C.

SDS-PAGE and immunoblotting

Total cells, immunoprecipitates, and EndoF1 digest reactions were taken up in SDS sample buffer and heated to 95°C for 10 min. Samples were separated on a 10-12% resolving SDS gel. For immunoblotting, the proteins were transferred to a polyvinylidene fluoride (PVDF) membrane, which was blocked with 5% dried milk in TBST (1.5 M NaCl, 0.1 M Tris-Cl, 0.05% Tween-20 at pH 7.4) for 1 h at room temperature. Primary and secondary antibodies were applied to the membranes for 1 hour at room temperature in TBST. In between and afterwards, the membrane was washed six times in TBST. Proteins were detected by enzyme-catalyzed fluorescence using a phosphor imager FLA 3000.

Flow cytometry

LCL 721.220 and LCL 721.221 cells expressing GFP fusions of B27 and B44 allotypes were incubated in 100 μL W6/32 hybridoma supernatant for 1 h on ice and washed with ice-cold PBS for three times. Cells were then incubated in allophycocyanin conjugated anti-mouse secondary antibody for 30 min on ice and washed with PBS for three times following the antibody incubation. Mean fluorescence intensity of GFP and allophycocyanin in each sample was recorded by a Partec CyFlowSpace flow cytometer (Münster, Germany). CMT64.5 cells were trypsinized and washed in PBS. A total of 2×10^6 cells were incubated in 100 μL W6/32 hybridoma supernant for 1 h on ice and washed three times in ice-cold PBS. Subsequently, the cells were stained with 6 μg/mL goat anti-mouse Alexa 488 in 50 μL PBS for 1 h on ice and washed again three times in ice-cold PBS. Samples were analyzed with a Partec CyFlowSpace flow cytometer (Münster, Germany) and processed with FlowJo (TreeStar, Ashland, OR, USA). To generate the plots in Fig. 6A, B as described previously [35, 44], we calculated the mean gene expression level (GFP) and mean antibody staining intensity (allophycocyanin) for each of the five sectors, which were generated by drawing four lines parallel to the allophycocyanin axis dividing the allophycocyanin versus GFP scatter plots in five consecutive areas that corresponded to different GFP fluorescence intensity ranges (Fig. 5C). We then plotted these mean values as the five data points shown in Fig. 6A, B for each transfectant.

Microscopy

Transfected LCL 721.220 cells were allowed to adhere onto glass cover slips at 37°C for 30 min and fixed with 3% paraformaldehyde (AppliChem, Darmstadt, Germany) for 20 min at room temperature. Staining was performed by monoclonal anti-HA antibody (clone 12CA5) and secondary antibody anti-mouse IgG coupled to Cy5 (Dianova, Hamburg, Germany). Cells were permeabilized with 0.05% Triton X-100 for 5 min at room temperature prior to staining of ER with calnexin antiserum (kind gift from David B. Williams, University of Toronto, Toronto, Canada) combined with anti-rabbit IgG-Cy3 (Dianova, Hamburg, Germany). B27 allotypes were visualized by anti-HA and secondary antibody anti-mouse conjugated with Alexa488. Cover slips were mounted onto glass slides, and confocal images were taken with a Zeiss LSM 510 microscope (Zeiss, Jena, Germany).

Acknowledgments: We thank Hartmut Hengel, Alain Townsend, and David Williams for reagents. Our work was supported by the Deutsche Forschungsgemeinschaft (SP583/2-3 and 8-1 to S.Sp.), the German Academic Exchange Service (to E.T.A.), and the TRC of Oman (RC/MED/MICR/14/1 to M.Al-B.).

Conflict of interest: The authors declare no commercial or financial conflict of interest.

References

1 **Yaneva, R., Schneeweiss, C., Zacharias, M. and Springer, S.**, Peptide binding to MHC class I and II proteins: new avenues from new methods. *Mol. Immunol.* 2010. **47**: 649–657.

2 **Reichen, C., Hansen, S. and Pluckthun, A.**, Modular peptide binding: from a comparison of natural binders to designed armadillo repeat proteins. *J. Struct. Biol.* 2014. **185**: 147–162.

3 **Lankat-Buttgereit, B. and Tampe, R.**, The transporter associated with antigen processing TAP: structure and function. *FEBS Lett.* 1999. **464**: 108–112.

4 **Blum, J. S., Wearsch, P. A. and Cresswell, P.**, Pathways of antigen processing. *Annu. Rev. Immunol.* 2013. **31**: 443-473.

5 **Wright, C. A., Kozik, P., Zacharias, M. and Springer, S.**, Tapasin and other chaperones: models of the MHC class I loading complex. *Biol. Chem.* 2004. **385**: 763–778.

6 **Lopez de Castro, J. A.**, HLA-B27 and the pathogenesis of spondyloarthropathies. *Immunol. Lett.* 2007. **108**: 27–33.

7 **Taurog, J. D.**, The mystery of HLA-B27: if it isn't one thing, it's another. *Arthritis Rheum.* 2007. **56**: 2478–2481.

8 **Khan, M. A.**, Update: the twenty subtypes of HLA-B27. *Curr. Opin. Rheumatol.* 2000. **12**: 235–238.

9 **Colbert, R. A., DeLay, M. L., Klenk, E. I. and Layh-Schmitt, G.**, From HLA-B27 to spondyloarthritis: a journey through the ER. *Immunol. Rev.* 2010. **233**: 181–202.

10 **Olivieri, I., Ciancio, G., Padula, A., Gaudiano, C., Masciandaro, S., Moro, L., Durante, E. et al.**, The HLA-B*2709 subtype confers susceptibility to spondylarthropathy. *Arthritis Rheum.* 2002. **46**: 553–554.

11 **Nasution, A. R., Mardjuadi, A., Kunmartini, S., Suryadhana, N. G., Setyohadi, B., Sudarsono, D., Lardy, N. M. and Feltkamp, T. E.**, HLA-B27 subtypes positively and negatively associated with spondyloarthropathy. *J. Rheumatol.* 1997. **24**: 1111–1114.

12 **D'Amato, M., Fiorillo, M. T., Carcassi, C., Mathieu, A., Zuccarelli, A., Bitti, P. P., Tosi, R. and Sorrentino, R.**, Relevance of residue 116 of HLA-B27 in determining susceptibility to ankylosing spondylitis. *Eur. J. Immunol.* 1995. **25**: 3199–3201.

13 **Kumar, P., Vahedi-Faridi, A., Saenger, W., Merino, E., Lopez de Castro, J. A., Uchanska-Ziegler, B. and Ziegler, A.**, Structural basis for T cell alloreactivity among three HLA-B14 and HLA-B27 antigens. *J. Biol. Chem.* 2009. **284**: 29784–29797.

14 **McHugh, K. and Bowness, P.**, The link between HLA-B27 and SpA—new ideas on an old problem. *Rheumatology* 2012. **51**: 1529–1539.

15 **Ziegler, A., Loll, B., Misselwitz, R. and Uchanska-Ziegler, B.**, Implications of structural and thermodynamic studies of HLA-B27 subtypes exhibiting differential association with ankylosing spondylitis. *Adv. Exp. Med. Biol.* 2009. **649**: 177–195.

16 **Ramos, M., Paradela, A., Vazquez, M., Marina, A., Vazquez, J. and Lopez de Castro, J. A.**, Differential association of HLA-B*2705 and B*2709 to ankylosing spondylitis correlates with limited peptide subsets but not with altered cell surface stability. *J. Biol. Chem.* 2002. **277**: 28749–28756.

17 **Lewis, J. W., Neisig, A., Neefjes, J. and Elliott, T.**, Point mutations in the alpha 2 domain of HLA-A2.1 define a functionally relevant interaction with TAP. *Curr. Biol.* 1996. **6**: 873–883.

18 **Zernich, D., Purcell, A. W., Macdonald, W. A., Kjer-Nielsen, L., Ely, L. K., Laham, N., Crockford, T. et al.**, Natural HLA class I polymorphism controls the pathway of antigen presentation and susceptibility to viral evasion. *J. Exp. Med.* 2004. **200**: 13–24.

19 **Simone, L. C., Georgesen, C. J., Simone, P. D., Wang, X. and Solheim, J. C.**, Productive association between MHC class I and tapasin requires the tapasin transmembrane/cytosolic region and the tapasin C-terminal Ig-like domain. *Mol. Immunol.* 2012. **49**: 628–639.

20 **Dong, G., Wearsch, P. A., Peaper, D. R., Cresswell, P. and Reinisch, K. M.**, Insights into MHC class I peptide loading from the structure of the tapasin-ERp57 thiol oxidoreductase heterodimer. *Immunity* 2009. **30**: 21–32.

21 **Garstka, M. A., Fritzsche, S., Lenart, I., Hein, Z., Jankevicius, G., Boyle, L. H., Elliott, T. et al.**, Tapasin dependence of major histocompatibility complex class I molecules correlates with their conformational flexibility. *FASEB J.* 2011. **25**: 3989–3998.

22 **Williams, A. P., Peh, C. A., Purcell, A. W., McCluskey, J. and Elliott, T.**, Optimization of the MHC class I peptide cargo is dependent on tapasin. *Immunity* 2002. **16**: 509–520.

23 **Praveen, P. V., Yaneva, R., Kalbacher, H. and Springer, S.**, Tapasin edits peptides on MHC class I molecules by accelerating peptide exchange. *Eur. J. Immunol.* 2010. **40**: 214–224.

24 **Geironson, L., Thuring, C., Harndahl, M., Rasmussen, M., Buus, S., Roder, G. and Paulsson, K. M.**, Tapasin facilitation of natural HLA-A and -B allomorphs is strongly influenced by peptide length, depends on stability, and separates closely related allomorphs. *J. Immunol.* 2013. **191**: 3939–3947.

25 **Peh, C. A., Burrows, S. R., Barnden, M., Khanna, R., Cresswell, P., Moss, D. J. and McCluskey, J.**, HLA-B27-restricted antigen presentation in the absence of tapasin reveals polymorphism in mechanisms of HLA class I peptide loading. *Immunity* 1998. **8**: 531–542.

26 **Park, B., Lee, S., Kim, E. and Ahn, K.**, A single polymorphic residue within the peptide-binding cleft of MHC class I molecules determines spectrum of tapasin dependence. *J. Immunol.* 2003. **170**: 961–968.

27 **Purcell, A. W., Gorman, J. J., Garcia-Peydro, M., Paradela, A., Burrows, S. R., Talbo, G. H., Laham, N. et al.**, Quantitative and qualitative influences of tapasin on the class I peptide repertoire. *J. Immunol.* 2001. **166**: 1016–1027.

28 **Paulsson, K. M., Kleijmeer, M. J., Griffith, J., Jevon, M., Chen, S., Anderson, P. O., Sjogren, H. O. et al.**, Association of tapasin and COPI provides a mechanism for the retrograde transport of major histocompatibility complex (MHC) class I molecules from the Golgi complex to the endoplasmic reticulum. *J. Biol. Chem.* 2002. **277**: 18266–18271.

29 **Sieker, F., Straatsma, T. P., Springer, S. and Zacharias, M.**, Differential tapasin dependence of MHC class I molecules correlates with conformational changes upon peptide dissociation: a molecular dynamics simulation study. *Mol. Immunol.* 2008. **45**: 3714–3722.

30 **Bouvier, M. and Wiley, D. C.**, Importance of peptide amino and carboxyl termini to the stability of MHC class I molecules. *Science* 1994. **265**: 398–402.

31 **Narzi, D., Becker, C. M., Fiorillo, M. T., Uchanska-Ziegler, B., Ziegler, A. and Bockmann, R. A.**, Dynamical characterization of two differentially disease associated MHC class I proteins in complex with viral and self-peptides. *J. Mol. Biol.* 2012. **415**: 429–442.

32 **Yaneva, R., Springer, S. and Zacharias, M.**, Flexibility of the MHC class II peptide binding cleft in the bound, partially filled, and empty states: a molecular dynamics simulation study. *Biopolymers* 2009. **91**: 14–27.

33 **Kienast, A., Preuss, M., Winkler, M. and Dick, T. P.**, Redox regulation of peptide receptivity of major histocompatibility complex class I molecules by ERp57 and tapasin. *Nat. Immunol.* 2007. **8**: 864–872.

34 **Klar, D. and Hammerling, G. J.**, Induction of assembly of MHC class I heavy chains with beta 2microglobulin by interferon-gamma. *EMBO J.* 1989. **8**: 475–481.

35 **Howe, C., Garstka, M., Al-Balushi, M., Ghanem, E., Antoniou, A. N., Fritzsche, S., Jankevicius, G. et al.**, Calreticulin-dependent recycling in the early secretory pathway mediates optimal peptide loading of MHC class I molecules. *EMBO J.* 2009. **28**: 3730–3744.

36 **Hulsmeyer, M., Hillig, R. C., Volz, A., Ruhl, M., Schroder, W., Saenger, W., Ziegler, A. and Uchanska-Ziegler, B.**, HLA-B27 subtypes differentially associated with disease exhibit subtle structural alterations. *J. Biol. Chem.* 2002. **277**: 47844–47853.

37 **Uranga, J., Mikulskis, P., Genheden, S. and Ryde, U.**, Can the protonation state of histidine residues be determined from molecular dynamics simulations? *Comput. Theoret. Chem.* 2012. **1000**: 75–84.

38 **Olsson, M. H. M., Sondergaard, C. R., Rostkowski, M. and Jensen, J. H.**, PROPKA3: consistent treatment of internal and surface residues in empirical pK(a) predictions. *J. Chem. Theory Comput.* 2011. **7**: 525–537.

39 **Badrinath, S., Saunders, P., Huyton, T., Aufderbeck, S., Hiller, O., Blasczyk, R. and Bade-Doeding, C.**, Position 156 influences the peptide repertoire and tapasin dependency of human leukocyte antigen B*44 allotypes. *Haematologica* 2012. **97**: 98-106.

40 **Beerbaum, M., Ballaschk, M., Erdmann, N., Schnick, C., Diehl, A., Uchanska-Ziegler, B., Ziegler, A. and Schmieder, P.**, NMR spectroscopy reveals unexpected structural variation at the protein-protein interface in MHC class I molecules. *J. Biomol. NMR* 2013. **57**: 167–178.

41 **Fussell, H., Nesbeth, D., Lenart, I., Campbell, E. C., Lynch, S., Santos, S., Gould, K. et al.**, Novel detection of in vivo HLA-B27 conformations correlates with ankylosing spondylitis association. *Arthritis Rheumatism* 2008. **58**: 3419–3424.

42 **Hulsmeyer, M., Welfle, K., Pohlmann, T., Misselwitz, R., Alexiev, U., Welfle, H., Saenger, W. et al.**, Thermodynamic and structural equivalence of two HLA-B27 subtypes complexed with a self-peptide. *J. Mol. Biol.* 2005. **346**: 1367–1379.

43 **Starikov, E. B., Nilsson, L. and Hulsmeyer, M.**, A single residue exchange between two HLA-B27 alleles triggers increased peptide flexibility. *Eur. Biophys. J.* 2004. **33**: 651–655.

44 **Hein, Z., Uchtenhagen, H., Abualrous, E. T., Saini, S. K., Janssen, L., Van Hateren, A., Wiek, C. et al.**, Peptide-independent stabilization of MHC class I molecules breaches cellular quality control. *J. Cell Sci.* 2014. **127**: 2885–2897.

45 **Kurimoto, E., Kuroki, K., Yamaguchi, Y., Yagi-Utsumi, M., Igaki, T., Iguchi, T., Maenaka, K. and Kato, K.**, Structural and functional mosaic nature of MHC class I molecules in their peptide-free form. *Mol. Immunol.* 2013. **55**: 393–399.

46 **Mear, J. P., Schreiber, K. L., Munz, C., Zhu, X., Stevanovic, S., Rammensee, H. G., Rowland-Jones, S. L. and Colbert, R. A.**, Misfolding of HLA-B27 as a result of its B pocket suggests a novel mechanism for its role in susceptibility to spondyloarthropathies. *J. Immunol.* 1999. **163**: 6665–6670.

47 **Colbert, R. A.**, HLA-B27 misfolding: a solution to the spondyloarthropathy conundrum? *Mol. Med. Today* 2000. **6**: 224–230.

48 **Ford, S., Antoniou, A., Butcher, G. W. and Powis, S. J.**, Competition for access to the rat major histocompatibility complex class I peptide-loading complex reveals optimization of peptide cargo in the absence of transporter associated with antigen processing (TAP) association. *J. Biol. Chem.* 2004. **279**: 16077–16082.

49 **Galocha, B. and deCastro, J. A.**, Folding of HLA-B27 subtypes is determined by the global effect of polymorphic residues and shows incomplete correspondence to ankylosing spondylitis. *Arthritis Rheum.* 2008. **58**: 401–412.

50 **Montserrat, V., Galocha, B., Marcilla, M., Vazquez, M. and deCastro, J. A. L.**, HLA-B*2704, an allotype associated with ankylosing spondylitis, is critically dependent on transporter associated with antigen processing and relatively independent of tapasin and immunoproteasome for maturation, surface expression, and T cell recognition: relationship to B*2705 and B*2706. *J. Immunol.* 2006. **177**: 7015–7023.

51 **Dangoria, N. S., DeLay, M. L., Kingsbury, D. J., Mear, J. P., Uchanska-Ziegler, B., Ziegler, A. and Colbert, R. A.**, HLA-B27 misfolding is associated with aberrant intermolecular disulfide bond formation (dimerization) in the endoplasmic reticulum. *J. Biol. Chem.* 2002. **277**: 23459–23468.

52 **Wei, M. L. and Cresswell, P.**, HLA-A2 molecules in an antigen-processing mutant cell contain signal sequence-derived peptides. *Nature* 1992. **356**: 443–446.

53 **Henderson, R. A., Michel, H., Sakaguchi, K., Shabanowitz, J., Appella, E., Hunt, D. F. and Engelhard, V. H.**, HLA-A2.1-associated peptides from a mutant cell line: a second pathway of antigen presentation. *Science* 1992. **255**: 1264–1266.

54 **Lauvau, G., Gubler, B., Cohen, H., Daniel, S., Caillat-Zucman, S. and van Endert, P. M.**, Tapasin enhances assembly of transporters associated with antigen processing-dependent and -independent peptides with HLA-A2 and HLA-B27 expressed in insect cells. *J. Biol. Chem.* 1999. **274**: 31349–31358.

55 **Anderson, K. S., Alexander, J., Wei, M. and Cresswell, P.**, Intracellular transport of class I MHC molecules in antigen processing mutant cell lines. *J. Immunol.* 1993. **151**: 3407–3419.

56 **Fukazawa, T., Hermann, E., Edidin, M., Wen, J., Huang, F., Kellner, H., Floege, J. et al.**, The effect of mutant beta 2-microglobulins on the conformation of HLA-B27 detected by antibody and by CTL. *J. Immunol.* 1994. **153**: 3543–3550.

57 **Wang, J., Yu, D. T. Y., Fukazawa, T., Kellner, H., Wen, J., Cheng, X. K., Roth, G., Williams, K. M. and Raybourne, R. B.**, A monoclonal-antibody that recognizes Hla-B27 in the context of peptides. *J. Immunol.* 1994. **152**: 1197–1205.

58 **Grandea, A. G., 3rd, Golovina, T. N., Hamilton, S. E., Sriram, V., Spies, T., Brutkiewicz, R. R., Harty, J. T. et al.**, Impaired assembly yet normal trafficking of MHC class I molecules in Tapasin mutant mice. *Immunity* 2000. **13**: 213–222.

59 **Garbi, N., Tiwari, N., Momburg, F. and Hammerling, G. J.**, A major role for tapasin as a stabilizer of the TAP peptide transporter and consequences for MHC class I expression. *Eur. J. Immunol.* 2003. **33**: 264–273.

60 **Purcell, A. W., Kelly, A. J., Peh, C. A., Dudek, N. L. and McCluskey, J.**, Endogenous and exogenous factors contributing to the surface expression of HLA B27 on mutant APC. *Hum. Immunol.* 2000. **61**: 120–130.

61 **Zarling, A. L., Luckey, C. J., Marto, J. A., White, F. M., Brame, C. J., Evans, A. M., Lehner, P. J. et al.**, Tapasin is a facilitator, not an editor, of class I MHC peptide binding. *J. Immunol.* 2003. **171**: 5287–5295.

62 **Anderson, K., Cresswell, P., Gammon, M., Hermes, J., Williamson, A. and Zweerink, H.**, Endogenously synthesized peptide with an endoplasmic reticulum signal sequence sensitizes antigen processing mutant cells to class I-restricted cell-mediated lysis. *J. Exp. Med.* 1991. **174**: 489–492.

63 **Zarling, A. L., Luckey, C. J., Mart, J. A., White, F. M., Lehner, P. J., Cresswell, P., Shabanowitz, J. et al.**, Tapasin is a facilitator, not an editor, of HLA-B8 peptide binding. *Faseb. J.* 2003. **17**: C120–C120.

64 **Bird, L. A., Peh, C. A., Kollnberger, S., Elliott, T., McMichael, A. J. and Bowness, P.**, Lymphoblastoid cells express HLA-B27 homodimers both intracellularly and at the cell surface following endosomal recycling. *Eur. J. Immunol.* 2003. **33**: 748–759.

65 **Williams, D. B., Swiedler, S. J. and Hart, G. W.**, Intracellular transport of membrane glycoproteins: two closely related histocompatibility antigens differ in their rates of transit to the cell surface. *J. Cell Biol.* 1985. **101**: 725–734.

66 **Rizvi, S. M., Salam, N., Geng, J., Qi, Y., Bream, J. H., Duggal, P., Hussain, S. K. et al.**, Distinct assembly profiles of HLA-B molecules. *J. Immunol.* 2014. **192**: 4967–4976.

67 **Case, D. A., Darden, T. A., Cheatham, T. E., III, Simmerling, C. L., Wang, J., Duke, R. E., Luo, R. et al.**, *AMBER 12*, University of California, San Francisco, CA, USA 2012.

68 **Jorgensen, W. L., Chandrasekhar, J., Madura, J. D., Impey, R. W. and Klein, M. L.**, Comparison of simple potential functions for simulating liquid water. *J. Chem. Phys.* 1983. **79**: 926–935.

69 **Darden, T., York, D. and Pedersen, L.**, Particle Mesh Ewald—an N.Log(N) method for Ewald sums in large systems. *J. Chem. Phys.* 1993. **98**: 10089–10092.

70 **Humphrey, W., Dalke, A. and Schulten, K.**, VMD: visual molecular dynamics. *J. Mol. Graph* 1996. **14**: 33–38, 27–38.

71 **Mihel, J., Sikic, M., Tomic, S., Jeren, B. and Vlahovicek, K.**, PSAIA—protein structure and interaction analyzer. *BMC Struct. Biol.* 2008. **8**: 21.

72 **DeLano, W. L.**, *The PyMOL Molecular Graphics System*. DeLano Scientific LLC, San Carlos, CA USA.

73 **Majoul, I., Straub, M., Hell, S. W., Duden, R. and Soling, H. D.**, KDEL-cargo regulates interactions between proteins involved in COPI vesicle traffic: Measurements in living cells using FRET. *Dev. Cell* 2001. **1**: 139–153.

Abbreviations: **AS**: ankylosing spondylitis · **β_2m**: beta-2 microglobulin · **GFP**: green fluorescent protein · **MD**: molecular dynamics · **RMSD**: root mean square deviation · **SASA**: solvent-accessible surface area · **TAP**: transporter associated with antigen processing

Full correspondence: Prof. Sebastian Springer, Department of Life Science and Chemistry, Jacobs University Bremen, Campus Ring 1, 28759 Bremen, Germany
Fax: +49-421-200-3249
e-mail: s.springer@jacobs-university.de

Received: 3/11/2014
Revised: 6/12/2014
Accepted: 19/1/2015
Accepted article online: 23/1/2015

